Reactive Power Compensation and Optimization Strategy for Grid-Interactive Cascaded Photovoltaic Systems

Liming Liu, *Senior Member, IEEE*, Hui Li, *Senior Member, IEEE*, Yaosuo Xue, *Senior Member, IEEE*, and Wenxin Liu, *Member, IEEE*

***Abstract*—Cascaded multilevel converter structure can be appealing for high-power solar photovoltaic (PV) systems thanks to its modularity, scalability, and distributed maximum power point tracking (MPPT). However, the power mismatch from cascaded individual PV converter modules can bring in voltage and system operation issues. This paper addresses these issues, explores the effects of reactive power compensation and optimization on system reliability and power quality, and proposes coordinated active and reactive power distribution to mitigate this issue. A vector method is first developed to illustrate the principle of power distribution. Accordingly, the relationship between power and voltage is analyzed with a wide operation range. Then, an optimized reactive power compensation algorithm (RPCA) is proposed to improve the system operation stability and reliability, and facilitate MPPT implementation for each converter module simultaneously. Furthermore, a comprehensive control system with the RPCA is designed to achieve effective power distribution and dynamic voltage regulation. Simulation and experimental results are presented to demonstrate the effectiveness of the proposed reactive power compensation approach in grid-interactive cascaded PV systems.**

***Index Terms*—Cascaded photovoltaic (PV) system, power–voltage distribution, reactive power compensation, unsymmetrical active power.**

I. Introduction

WORLDWIDE renewable energy resources, especially solar energy, are growing dramatically in view of energy shortage and environmental concerns [1]–[3]. Large-scale solar photovoltaic (PV) systems are typically connected to medium-voltage distribution grids, where power converters are required to convert solar energy into electricity in such a grid-interactive PV system [4]–[14]. To achieve direct medium-voltage grid access without using bulky medium-voltage transformer, cascaded multilevel converters are attracting more and more attraction due to their unique advantages such as enhanced energy harvesting capability implemented by distributed maximum power point tracking (MPPT), improved energy efficiency, lower cost, higher power density, scalability and modularity, plug-N-power operation, etc. [11]–[14].

Although cascaded multilevel converters have been successfully introduced in medium- to high-voltage applications such as large motor drives, dynamic voltage restorers, reactive power compensations, and flexible ac transformation system devices [15]–[28], their applications in PV systems still face tough challenges because of solar power variability and the mismatch of maximum power point from each converter module due to manufacturing tolerances, partial shading, dirt, thermal gradients, etc. In a cascaded PV system, the total ac output voltage is synthesized by the output voltage from each converter module in one phase leg, which must fulfill grid codes or requirements. Ideally, each converter module delivers the same active power to grid; hence, symmetrical voltage is distributed among these modules. However, in the event of active power mismatch from these modules, the converter module with higher active power generation will carry more proportion of the whole ac output voltage, which may result in overmodulation if the system is not oversized design. In serious scenario, the synthesized output voltage may not be enough to meet the system requirement. As a result, the active power mismatch may not only result in losses in energy harvesting but also system instability and unreliability due to the inadequate output voltage or overmodulation issues.

Motivations aretoward addressing the aforementioned issues and approaching to mitigate the negative effect of active power mismatch. In [29]–[31], MPPT is achieved for each module in these approaches to enhance energy harvesting. However, only unity power factor control was considered and the inherent reactive power compensation capability of the cascaded PV system is ignored. As a result, the PV system still surfers from the degraded power quality and system reliability. It is recognized that reactive power compensation is able to provide strong voltage support in a wide range [18], [32]. Proper reactive power compensation can significantly improve the system reliability, and in the meantime help the MPPT implementation for the cascaded module under unsymmetrical condition as well as comply with the system voltage requirement simultaneously. All of these have spurred growing interest in reactive power compensation for the cascaded PV system. A reactive power compensation strategy is integrated in the control system of the cascaded PV system in [33]. However, this approach fails to consider the effect of voltage or current distortion caused by unsymmetrical active power on the power detection and distribution, and

Manuscript received September 24, 2013; revised November 26, 2013, March 31, 2014, and May 11, 2014; accepted October 31, 2013. Date of publication June 25, 2014; date of current version August 26, 2014. Recommended for publication by Associate Editor M. A. Perez.

L. Liu and H. Li are with the Center for Advanced Power Systems, Florida State University, Tallahassee, FL 32310 USA (e-mail: Limingcaps@gmail.com; Hlicaps@gmail.com).

Y. Xue is with Siemens Corporate Research, Princeton, NJ 08540 USA (e-mail: Yaosuo.xue@siemens.com).

W. Liu is with the New Mexico State University, Las Cruces, NM 88003 USA (e-mail: Wliu@nmsu.edu).

Color versions of one or more of the figures in this paper are available online at http://ieeexplore.ieee.org.

Digital Object Identifier 10.1109/TPEL.2014.2333004

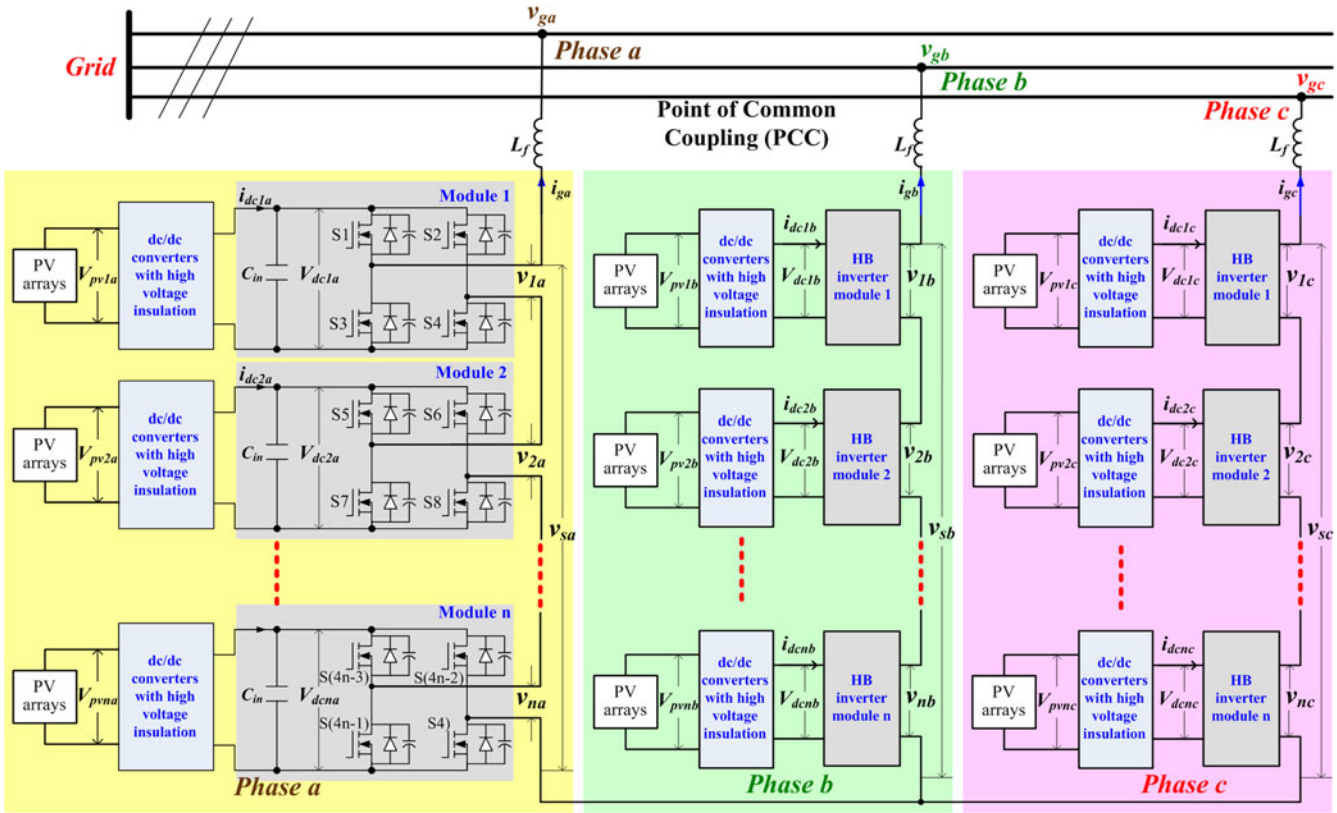

Fig. 1. Grid-interactive PV system with cascaded PV converters.

the converter module with high active power generation is not required to provide reactive power, which has limited the capability of reactive power compensation. Therefore, optimized solutions have yet to be found and it is very critical to develop an effective reactive power compensation strategy for the grid-interactive cascaded PV system.

This paper proposes an optimized reactive power compensation method and evaluates the effect of reactive power compensation on system reliability and power quality in the grid-interactive PV system with cascaded converter modules. A proper reactive power compensation and distribution is considered to eliminate the overmodulation caused by unsymmetrical active power. In the proper reactive power management, one first emphasizes that the output voltage from the cascaded PV system must to meet the grid code. The maximum reactive power compensation will be activated to mitigate this issue once active power mismatch occurs and voltage and current distortion are detected. In this way, correct active and reactive power can be calculated, and MPPT for each module can be achieved and grid code can be met simultaneously. However, overcompensation of reactive power may be provided, which increases the system burden. Therefore, reactive power compensation among modules is optimized and redistributed considering their respective active power contribution on the premise that MPPT can be achieved and grid code is fulfilled. As a result, the system reliability will be enhanced.

The rest of this paper is organized as follows. In Section II, the cascaded PV system configuration is presented and a vector diagram is first derived to help illustrate the principle of active and reactive power distribution between each module. Correspondingly, the relationship between power and output voltage for each module is analyzed under different conditions. A reactive power compensation algorithm (RPCA), which is inherently suitable for different types of cascaded PV system, is developed in Section III to improve system operation performance in view of point of common coupling (PCC) voltage range and MPPT implementation. Accordingly, a control system with the proposed RPCA is designed to achieve dynamic voltage regulation and optimized power distribution. The proposed reactive power compensation method is implemented in the MATLAB/Simulink and PSIM cosimulation platform and a 10 kVA grid-interactive laboratory prototype. Simulation and experimental results at 2 kVA are given to confirm the validity of the proposed reactive power compensation method in Sections IV and V, respectively, followed by conclusion in Section VI.

II. System Configuration and Power–Voltage Distribution

A. System Configuration

Fig. 1 describes the system configuration of one two-stage grid-interactive PV system with n cascaded converter modules for each phase, which is very suitable for the medium/high voltage application. It can be immune to the leakage current and PV potential induced degradation issues. In this paper, three-phase PV converters are connected in "wye" configuration. They

TABLE I
VARIABLE DESCRIPTION IN FIG. 1

Symbol	Definition
V_{pvjt} $(j = 1, 2, \ldots, n; t = a, b, c)$	output voltage from each PV arrays
V_{dcjt}	dc capacitor voltage
i_{dcjt}	dc current
v_{gt}	grid voltage on point of common coupling (PCC)
i_{gt}	grid current
v_{st}	converter output voltage from each phase
v_{jt}	output voltage from each module
C_{in}	dc capacitor
L_f	grid filter inductor

also can be connected in "delta" configuration. The variables in Fig. 1 are defined in Table I.

In the two-stage PV system, the first-stage dc/dc converters with high voltage insulation can achieve the voltage boost and MPPT for the segmented PV arrays [34], [35]. The second-stage three-level H-bridge converter modules are cascaded to augment the output voltage, deliver active power to grid, and provide reactive power compensation. The dc-link voltage can be controlled to be constant and the same in each converter module. For the low voltage application, single-stage system configuration can be considered, where the dc/dc converters in Fig. 1 can be replaced by Quasi-Z-Source network or be removed according to system requirement [7], [29], [30], [32]. The single-stage PV system features simple configuration and fewer devices integration in each module. However, additional methods need be developed to solve the leakage current issues. In addition, the system may need to be oversized to accommodate the wide input voltage variation [25], [30], [32]. In these configurations, unsymmetrical active power may be harvested from the cascaded modules due to PV module mismatch, orientation mismatch, partial shading, etc. In this case, improper power distribution and control are prone to an intrinsic instability problem if MPPT is still desired, which results in a limited operation range for the system [36]. Moreover, it may also seriously deteriorate the system reliability and power quality. Particularly, appropriate reactive power compensation is very helpful to improve the operation of the cascaded PV system. Considering active power is produced by PV arrays and reactive power injection or absorption is regardless of PV arrays, one expects an independent active and reactive power control for each module. By this way, effect of reactive power compensation on system reliability and power quality can be investigated. In this paper, efforts are focused on the intelligent reactive power compensation method and optimized reactive power distribution from each module.

B. Power and Voltage Distribution Analysis

In the cascaded PV system, the same ac grid current flows through the ac side of each converter module. Therefore, the output voltage distribution of each module will determine the active and reactive power distribution. In order to clarify the power distribution, four modules are selected in the cascaded PV converters in each phase as an example. Vector diagrams are derived in Fig. 2 to demonstrate the principle of power distribution between the cascaded converter modules in phase a [14]. The same analysis can be extended to phases b and c. It means that active and reactive power will be independently controlled in each phase. Therefore, a discrete Fourier transform phase-locked loop (PLL) method is adopted in this paper, which is only based on single-phase grid voltage orientation and can extract fundamental phase, frequency, and amplitude information from any signal [8]. Considering that the PCC voltage is relatively stable, v_{ga} is first used as the PLL synchronous signal of the cascaded PV system as shown in Fig. 2(a). v_{ga} is transformed into $\alpha\beta$ stationary reference frame quantities v_{ga_α} and v_{ga_β} which is the virtual voltage with $\pi/2$ phase shift to v_{ga_α}. They are converted to v_{ga_d} and v_{ga_q} in the dq synchronous reference frame, where v_{ga} is aligned with the d-axis by PLL control [8]. Ideally, v_{ga_d} is equal to the magnitude of PCC voltage V_{ga} and v_{ga_q} is zero. Once the phase-shift angle θ_{iga} between v_{ga} and grid current i_{ga} is detected, the new $d'q'$ synchronous reference frame can be defined. In this frame, i_{ga} is aligned with the d'-axis. Therefore, the d'-axis component $v_{sa\_d'}$ of the whole PV system output voltage v_{sa} directly decides the active power injection. The contribution of each module output voltage on q'-axis component $v_{sa\_q'}$ is closely related to the reactive power compensation.

Fig. 2(b) illustrates voltage distribution of four cascaded converter modules under unsymmetrical active power generation in phase a. The output voltage of the total converter V_{sa} is synthesized by the four converter module output voltage with different amplitude and angles. The voltage components of each module in $d'q'$ frame, $v_{ja\_d'}$ and $v_{ja\_q'}$ $(j = 1, 2, \ldots, 4)$, can be independently controlled to implement the decoupled active and reactive power control. Because of the same grid current through each convert module, the distributed d'-axis and q'-axis voltage components in $d'q'$ frame determine the active and reactive power distribution in these converter modules, respectively. The $v_{1a\_d'} > v_{2a\_d'} > v_{3a\_d'} > v_{4a\_d'}$ indicates that module 1 generates the maximum active power and module 4 generates the minimum active power. The $v_{1a\_q'} = v_{2a\_q'} = v_{3a\_q'} = v_{4a\_q'}$ reveals that the same reactive power is provided by these modules. The previous analysis further clarified the relationship between the previous voltage components and power distribution.

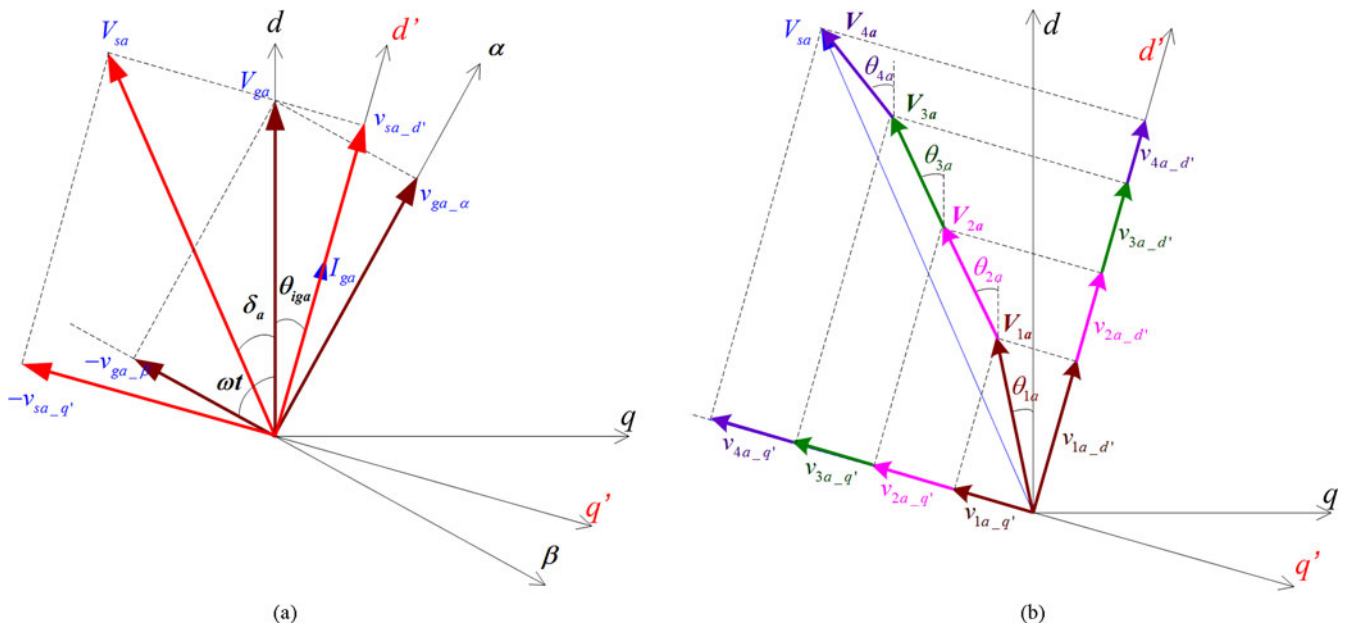

Fig. 2. Vector diagrams showing relation between $\alpha\beta$ frame, dq frame, and $d'q'$ frame. (a) Relationship between grid current, grid voltage, and converter output voltage in phase a. (b) Voltage distribution of the PV converter in phase a.

The average active and reactive power to grid in phase a, P_{ga} and Q_{ga}, can be derived by

$$P_{ga} - jQ_{ga} = \vec{V}_{ga}\left(\frac{\vec{V}_{sa} - \vec{V}_{ga}}{jX_L}\right)^* \tag{1}$$

where $\vec{V}_{ga}$ is the vector of v_{ga}, $\vec{V}_{sa}$ is the vector of v_{sa}, $X_L = \omega L_f$, ω is the fundamental radian frequency, and L_f is the grid filter inductor.

Considering the cascaded topology and modular structure, P_{ga} and Q_{ga} can also be expressed as

$$\begin{cases} P_{ga} = \frac{1}{2}\frac{V_{sa}V_{ga}}{X_L}\sin\delta_a = \frac{1}{2}V_{ga}i_{ga\_d} \\ \quad = \frac{1}{2}v_{sa\_d'} \times \sqrt{i_{ga\_d}^2 + i_{ga\_q}^2} \\ Q_{ga} = -\frac{1}{2}\frac{V_{sa}V_{ga}}{X_L}\cos\delta_a + \frac{1}{2}\frac{V_{ga}^2}{X_L} = \frac{1}{2}V_{ga}i_{ga\_q} \\ \quad = \frac{1}{2}v_{sa\_q'} \times \sqrt{i_{ga\_d}^2 + i_{ga\_q}^2} + \frac{1}{2}\left(i_{ga\_d}^2 + i_{ga\_q}^2\right)X_L \end{cases} \tag{2}$$

where V_{ga} is the magnitude of v_{ga}, V_{sa} is the magnitude of v_{sa}, δ_a is phase angle between v_{ga} and v_{sa}, i_{ga_d} is the d-axis component of i_{ga}, and i_{ga_q} is the q-axis component of i_{ga}.

In order to evaluate the effect of reactive power compensation on the system reliability, one assumes that P_{ga} and Q_{ga} in the general case are given by

$$\begin{cases} P_{ga} = k_1 P_{ga\_\text{rated}} = \frac{1}{2}k_1 V_{ga} i_{ga\_d\_\text{rated}} \\ \quad = \frac{1}{2}\sqrt{k_1^2 + k_2^2}\, v_{sa\_d'} i_{ga\_d\_\text{rated}} \\ Q_{ga} = k_2 Q_{ga\_\text{rated}} = k_2 P_{ga\_\text{rated}} = \frac{1}{2}k_2 V_{ga} i_{ga\_d\_\text{rated}} \\ \quad = \frac{1}{2}\sqrt{k_1^2 + k_2^2}\, v_{sa\_q'} i_{ga\_d\_\text{rated}} \\ \qquad + \frac{1}{2}\left(k_1^2 + k_2^2\right) i_{ga\_d\_\text{rated}}^2 X_L \end{cases} \tag{3}$$

where P_{ga_rated} is the rated active power to grid in phase a, Q_{ga_rated} is the rated reactive power to grid in phase a and numerically equal to P_{ga_rated}, $i_{ga\_d\_\text{rated}}$ is the d-axis component of rated grid current in phase a, and $k1$ and $k2$ are defined as active and reactive power distribution coefficients, respectively.

According to (2) and (3), V_{sa} can be calculated as

$$\begin{aligned} V_{sa} &= \sqrt{v_{sa\_d'}^2 + v_{sa\_q'}^2} \\ &= \sqrt{\left(\frac{2k_1 P_{ga\_\text{rated}} X_L}{V_{ga}}\right)^2 + \left(\frac{2k_2 P_{ga\_\text{rated}} X_L}{V_{ga}} - V_{ga}\right)^2}. \end{aligned} \tag{4}$$

Based on (3), the $v_{sa\_d'}$ and $v_{sa\_q'}$ can be derived by

$$\begin{cases} v_{sa\_d'} = \frac{k_1}{\sqrt{k_1^2 + k_2^2}} V_{ga} \\ v_{sa\_q'} = \frac{k_2}{\sqrt{k_1^2 + k_2^2}} V_{ga} - \sqrt{k_1^2 + k_2^2}\, i_{ga\_d\_\text{rated}} X_L. \end{cases} \tag{5}$$

A specific PV system application is selected to illustrate the relationship between active power, reactive power, and output voltage as shown in Figs. 3–6. In this application, the P_{ga_rated} is 1 MW, L_f is 0.8 mH, and the root mean square (RMS) value of line-line PCC voltage is 12 kV. V_{sa}, $v_{sa\_d'}$, and $v_{sa\_q'}$ are normalized to clarify the aforementioned analysis, which the magnitude of phase-ground PCC voltage V_{ga} is defined as 1.0 p.u.

Figs. 3 and 4 illustrate the operation range of $v_{sa\_d'}$ and $v_{sa\_q'}$ with k_1 and k_2 variation. Considering the PCC voltage regulation, k_2 may vary from -1 to 1 to achieve a wide range bidirectional reactive power compensation under a certain active power. Fig. 5 represents the operation range of V_{sa} with varied k_1 and k_2. Typically, V_{sa} is very close to V_{ga} when the filter inductor X_L is small. In order to verify the aforementioned

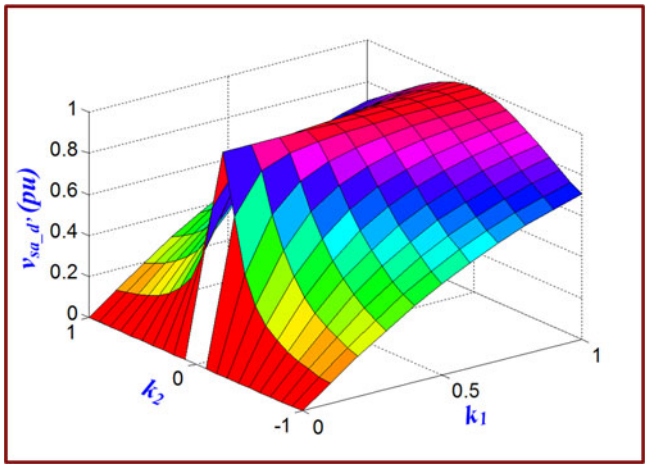

Fig. 3. Operation range of $v_{sa\_d'}$ with respect to different active and reactive power to grid.

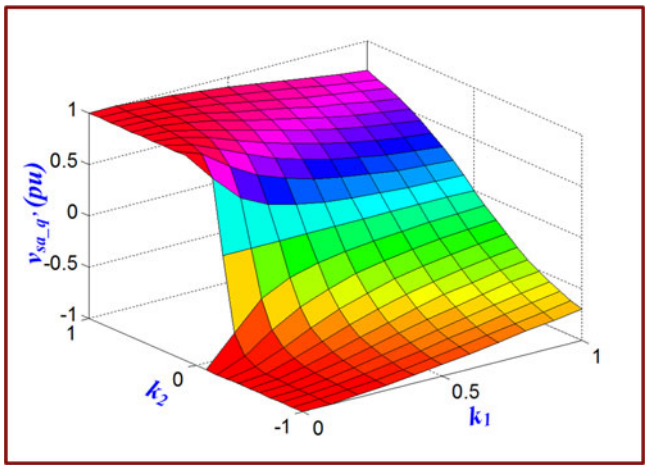

Fig. 4. Operation range of $v_{sa\_q'}$ with respect to different active and reactive power to grid.

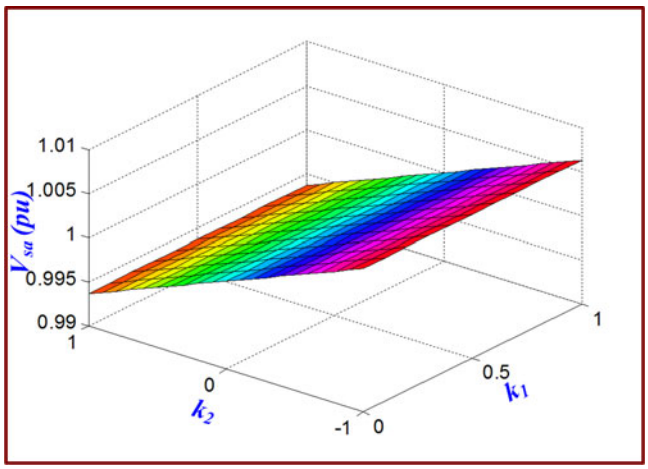

Fig. 5. Operation range of V_{sa} with respect to different active and reactive power to grid.

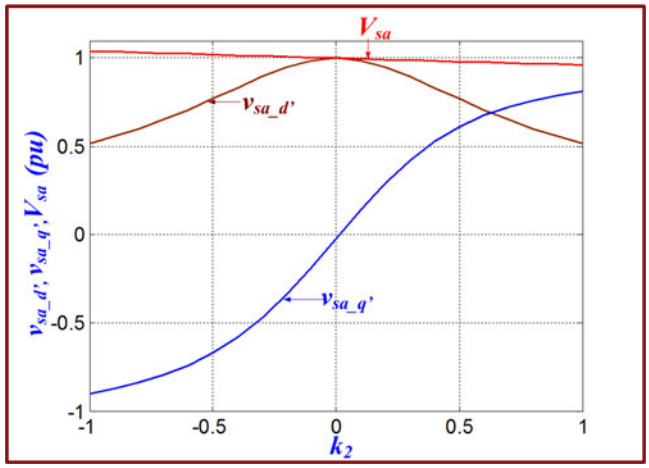

Fig. 6. Relationship between $v_{sa\_d'}$, $v_{sa\_q'}$, and V_{sa} with fixed $k_1 = 0.6$ and varied k_2.

analysis further, the relationship between $v_{sa\_d'}$, $v_{sa\_q'}$, and V_{sa} with fixed $k_1 = 0.6$ and varied k_2 is depicted in Fig. 6 as an example. There are different cases to generate active power with 0.6 P_{ga_rated} from the cascaded converter modules, where $v_{sa\_d'}$ and $v_{sa\_q'}$ change with k_2. No matter what kind of case, V_{sa} must fulfill the system requirement, which should be on the flat surface shown in Fig. 5.

It can be seen from Fig. 6 that $v_{sa\_d'}$ is gradually reduced with the increase of reactive power. The reduced $v_{sa\_d'}$ is helpful to reduce the burden of dc voltage. Fig. 7 shows an example with four cascaded converter modules to illustrate how reactive power compensation contributes to overcoming overmodulation caused by unsymmetrical active power in phase a. As shown in Fig. 7(a), the output voltages from four modules are the same under symmetrical active power generation, that is $V_{1a} = V_{2a} = V_{3a} = V_{4a}$. Their d'-axis components are also the same, which is $v_{1a\_d'} = v_{2a\_d'} = v_{3a\_d'} = v_{4a\_d'}$. There is no reactive power requirement. These output voltage, $V_{1a} - V_{4a}$, are not more than their respective dc voltage. However, when the unsymmetrical active power is produced by these modules, for example, the active power from modules 1 and 2 is greater than ones from modules 3 and 4, over-modulation will happen. As depicted in Fig. 7(b), $v_{1a\_d'}$ and $v_{2a\_d'}$ are greater than $v_{3a\_d'}$ and $v_{4a\_d'}$ considering the same ac current goes through these modules. Without reactive power compensation, V_{1a} and V_{2a} will exceed their dc voltage, which results in overmodulation of the two modules output voltages. With the help of reactive power, V_{1a} and V_{2a} are brought back to the desired values, which are less than their dc voltage as shown in Fig. 7(c). The increase of $v_{sa\_q'}$ contribute to the reduction of $v_{sa\_d'}$, which ensures that the synthesized voltage of each module by their d'-axis and q'-axis components is no more than dc voltage. Therefore, the overmodulation caused by unsymmetrical active power can be overcome.

It is obvious that the system reliability can be further enhanced if the reactive power compensation with a wider range is allowed by grid codes. When $k_2 < 0$, the PV system injects

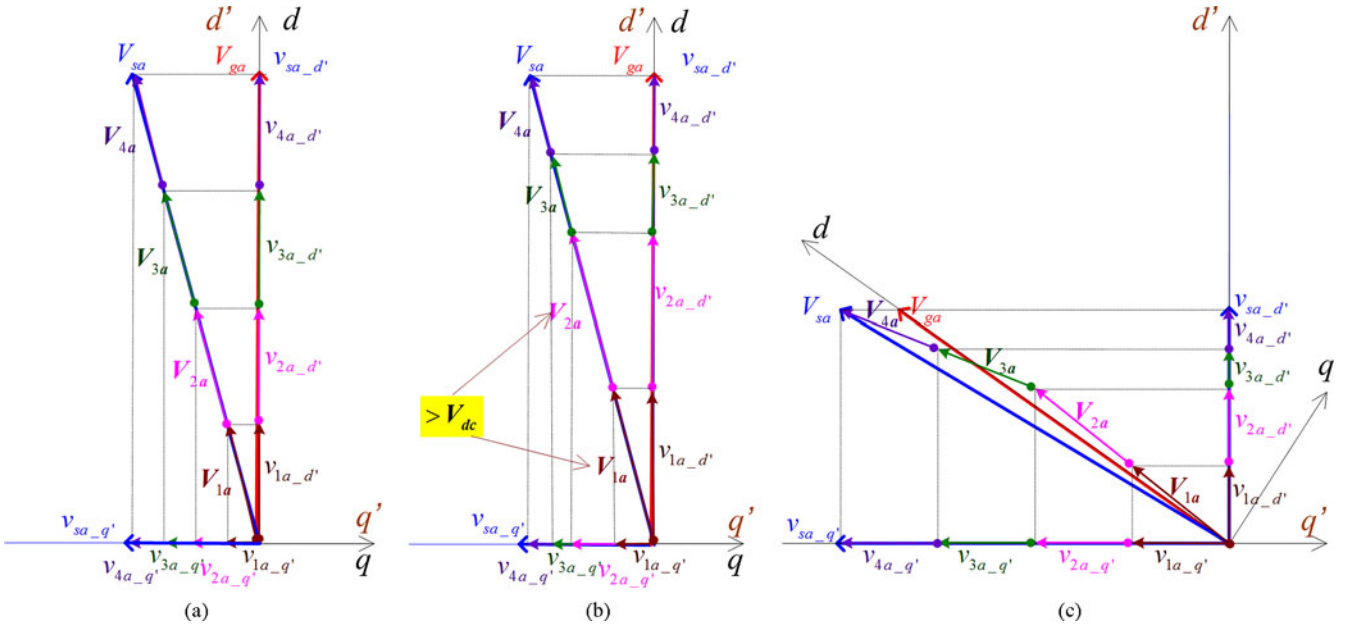

Fig. 7. Voltage distribution of four cascaded converter modules in $d'q'$ frame. (a) Symmetrical active power generation without reactive power compensation. (b) Unsymmetrical active power generation without reactive power compensation. (c) Unsymmetrical active power generation with reactive power compensation.

reactive power into grid to support PCC voltage to avoid undervoltage and help MPPT implementation. When $k_2 > 0$, the PV system absorbs reactive power from grid to support PCC voltage to avoid overvoltage and help MPPT implementation. However, if reactive power compensation is not allowed by grid codes, MPPT control will be disabled and equal active power output from each converter module will be controlled to ensure the reliable system operation, which will be introduced in Section III.

As discussed earlier, the objective of reactive power compensation is to avoid the overmodulation. In terms of the contribution of each module on $v_{sa\_d'}$ and $v_{sa\_q'}$, as well its dc link voltage, the output voltage of each PV converter module should be subject to the following constraint:

$$\sqrt{\left(m_{Pja}v_{sa\_d'}\right)^2 + \left(m_{Qja}v_{sa-q'}\right)^2} \le V_{dcja} \; (j = 1, 2, \ldots, n) \tag{6}$$

where m_{Pja} is defined as the percentage of $v_{sa\_d'}$ in the *j*th cell, m_{Qja} is defined as the percentage of $v_{sa\_q'}$ in the *j*th cell, $m_{Pa} = \sum_{j=1}^{n} m_{Pja} = 1$, $m_{Qa} = \sum_{j=1}^{n} m_{Qaj} = 1$, and V_{dcja} is the dc-link voltage in the *j*th cell in phase a.

An optimized RPCA will be elaborated in Section III. Fig. 8, as an instance, illustrates how to obtain an optimized voltage distribution related to reactive power distribution when the previous active power mismatch with $k_1 = 0.6$ happens as shown in Fig. 6, that is $m_{P1a} = m_{P2a} = 0.42$ and $m_{P3a} = m_{P4a} = 0.08$ in (6). It can be seen from Fig. 8(a) that the available range of reactive power compensation is $k_2 \in [-1, -0.6]$ when reactive power is injected into grid. There is no solutions satisfying the condition (6) for $k_2 \in [-0.6, 0]$, where $m_{Q1a} = m_{Q2a} = 0$ or $m_{Qa} < 1$ will both result in overmodulation. Considering the grid voltage, dc voltage ripple, and reactive power loss, the optimized voltage distribution at $k_2 = -0.6$ is selected as $m_{Q1a} = m_{Q2a} = 0.15$ and $m_{Q3a} = m_{Q4a} = 0.35$. Similarly, it can be seen from Fig. 8(b) that the available range of reactive power compensation is $k_2 \in [0.58, 1]$ when reactive power is absorbed by the cascaded PV system. There are no solutions satisfying the condition (6) for $k_2 \in [0, 0.58]$. Considering the grid voltage, dc voltage ripple, and reactive power loss, an optimized voltage distribution at $k_2 = 0.7$ is selected as $m_{Q1a} = m_{Q2a} = 0.15$ and $m_{Q3a} = m_{Q4a} = 0.35$.

In this way, the reactive power distribution and compensation can be optimized. The MPPT for each converter module and improved system reliability can be implemented simultaneously even under the unsymmetrical active power generation. Although the previous analysis is specified in phase a, the same analysis can be applied in phases b and c.

III. Proposed Reactive Power Compensation Method

A. RPCA

As aforementioned, appropriate reactive power compensation will enhance the cascaded PV system reliability and improve power quality, especially for unsymmetrical active power generation. Fig. 9 shows the proposed RPCA for the cascaded PV system in phase a. The same algorithm can be used in phases b and c. The reactive power compensation requirement Q_{ga}^* is associated with modulation index of output voltage from cascaded PV converter modules, PCC voltage, and MPPT control implementation which will determine the active power reference P_{ga}^*. In the initial state, MPPT control for each PV converter module is enabled and unity power factor is implemented considering symmetrical operation condition acts on these cascaded modules. In this scenario, Q_{ga}^* is zero and P_{ga}^* is derived from the sum of maximum active power from the individual PV

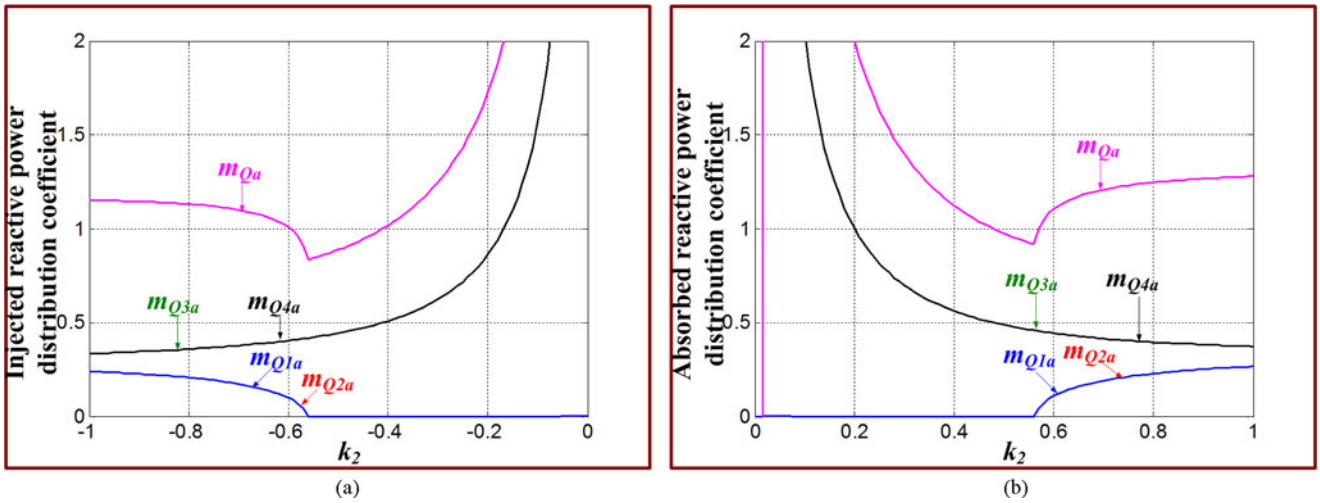

Fig. 8. Voltage distribution among four cascaded converter modules with $k_1 = 0.6$ and k_2 changes. (a) Reactive power injection. (b) Reactive power absorption.

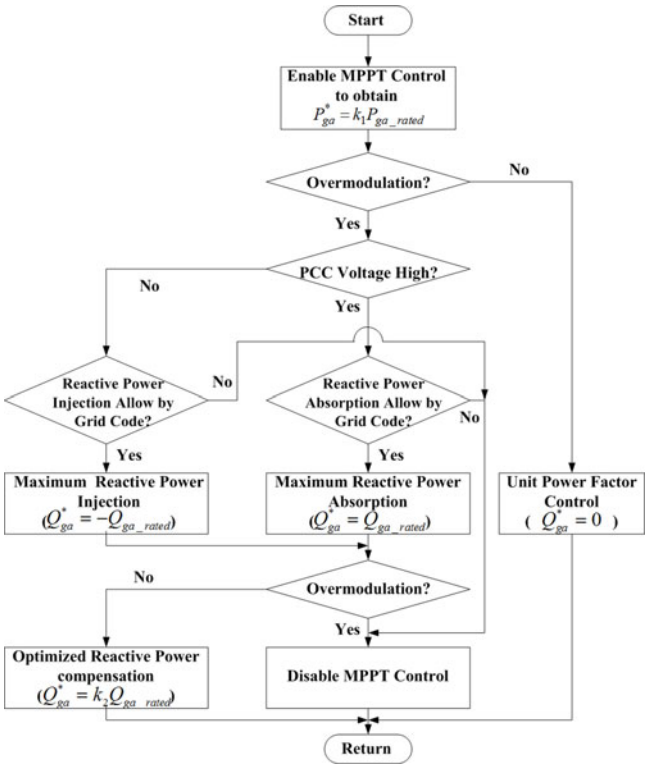

Fig. 9. Flowchart of the proposed RPCA.

arrays $\sum_{j=1}^{n} P_{pvja}$ subtracting power loss, which is defined as $k_1 P_{ga\_\mathrm{rated}}$. Considering the known P_{ga_rated}, k_1 can be calculated as $P^*_{ga}/P_{ga\_\mathrm{rated}}$. It is determined by the MPPT control and dc voltage control, which will be introduced in Section III-B. During the system operation, unsymmetrical active power may be generated from these modules due to PV module mismatch, orientation mismatch, partial shading, etc. As a result, overmodulation may occur on the PV converters output voltage, especially for the converter module with higher active power output, which seriously impairs the MPPT of each module and system reliability. Once the overmodulation is identified, the intentional reactive power compensation is activated to mitigate the overmodulation with grid code authorization. If PCC voltage is high, maximum reactive power will be absorbed from grid to bring down the PCC voltage with the normal voltage range according to the IEEE Std. 1547, as well help possible MPPT implementation for each converter module simultaneously. $k_2 = 1$ is designated to achieve the maximum reactive power absorption. The PV system operates like an inductor. Otherwise, the maximum reactive power is injected into grid to provide the PCC voltage support. $k_2 = -1$ is designated to execute the maximum reactive power injection. The PV system operates like a capacitor. If the maximum reactive power compensation still cannot eliminate the overmodulation, MPPT control will be disabled to ensure the security and stability of the cascaded PV system. Instead, reactive power compensation can be optimized, that is the selection of k_2, to reduce the risk of overvoltage or undervoltage caused by the maximum reactive power compensation. There are different ways to optimize reactive power distribution in the cascaded PV converter modules [14], [33]. In either way, the limited condition as shown in (6) must be satisfied to avoid the overmodulation. It is noted that the selected dc voltage and allowed voltage ripple will also impact on the reactive power compensation optimization. In this paper, the boundary condition in (6) is selected to achieve the optimized reactive power distribution, which can limit the unity modulation voltage output for the converter module with high active power generation, even help to possible equivalent apparent power being extracted from each PV converter module. The selection of k_2 is related to k_1 and the level of unsymmetrical active power, which can be obtained based on Fig. 8 and (6). A specific example in Fig. 8 will be provided to demonstrate the proposed RPCA in Section II.

B. Control System Design

A cascaded PV control system with the proposed RPCA in phase a is depicted in Fig. 10. The same control system is applied

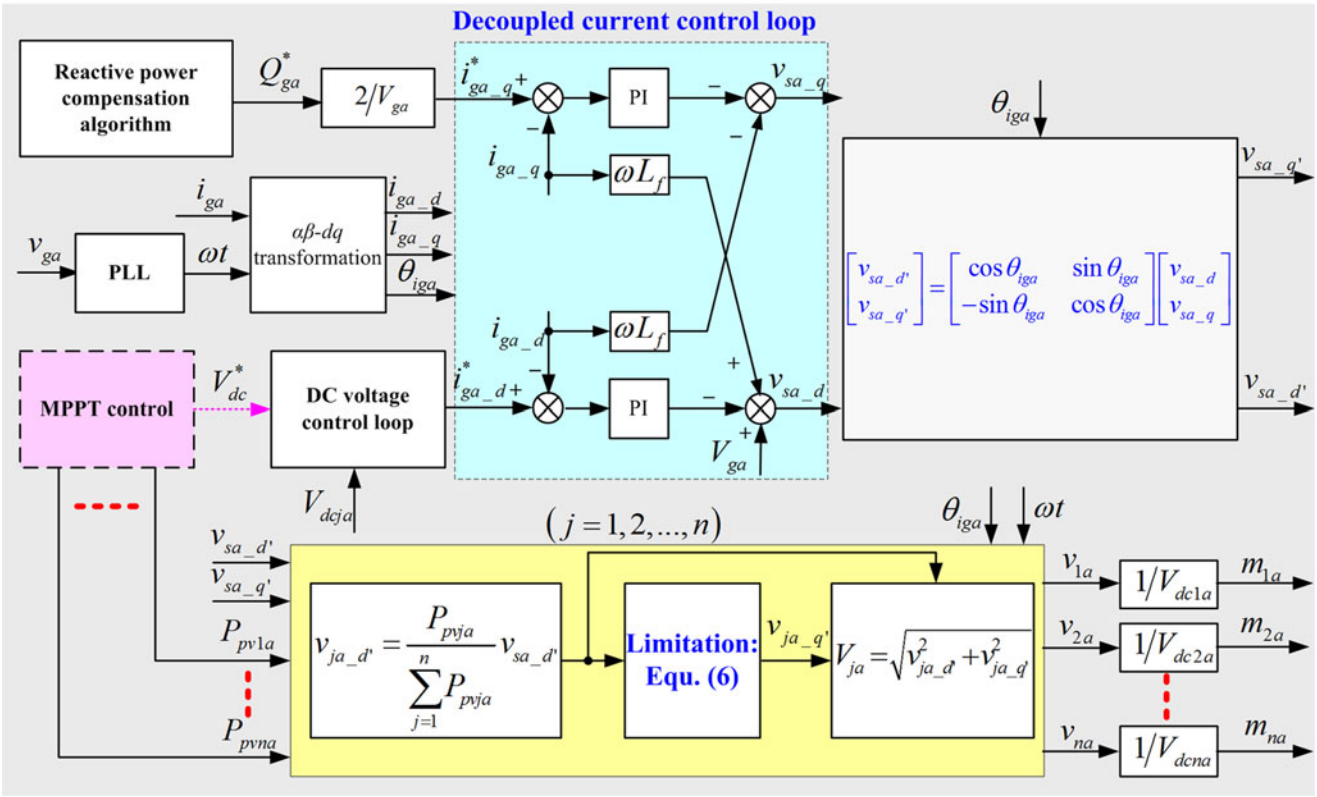

Fig. 10. Block diagram of cascaded PV control system with the proposed RPCA in phase a.

TABLE II
SYSTEM CIRCUIT PARAMETERS IN SIMULATION

	Parameters	Symbol	Value
PV converter modules in each phase	Number	n	4
	Capacitor voltage	$V_{dcki}(k=1,2\ldots n;t=a,b,c)$	3000 V (1.0 p.u.)
	Capacitor size	C_{in}	1000 μF (0.026 p.u.)
	Filter inductor	L_f	5 mH (0.056)
	Switching frequency for each device	f_{SW}	5 kHz
Grid (each phase)	Rated real power	P_{gt}_rated(t = a, b, c)	1 MW (0.333 p.u.)
	Rated reactive power	Q_{gt}_rated(t = a, b, c)	1 MVAR (0.333 p.u.)
	Rated RMS line–line voltage	V_{gL-L}	12 kV (1.0 p.u.)
	Rated phase-ground voltage magnitude	$V_{gt}(t=a,b,c)$	9.8 kV (0.817 p.u.)

in phases b and c. Particularly, the proposed PRCA can be applied for any type of the cascaded PV system, such as single-stage and two-stage PV system [7], [14], [30]. The active and reactive power is regulated in the *dq* synchronous reference frame. PLL is used to synchronize the output voltage of the cascaded PV converters v_{sa}, grid current i_{ga} with v_{ga} so that the desired power control can be achieved. The RPCA provides the desired reactive power Q^*_{ga} during unsymmetrical active power from the cascaded PV converter modules. The *q*-axis component command of grid current $i^*_{ga\_q}$ can be derived from the desired Q^*_{ga}. The maximum active power harvesting from each module can be implemented by MPPT control and dc-link voltage control. In the one-stage cascaded PV system, the dc-link voltage reference $V^*_{\rm dc}$ is obtained by the MPPT control for individual PV arrays. In the two-stage cascaded PV system, $V^*_{\rm dc}$ is designated based on the grid voltage requirement. The $V_{{\rm dc}ja}$ on each PV converter module is controlled to track $V^*_{\rm dc}$ to generate the *d*-axis component command of grid current $i^*_{ga\_d}$, which will coordinate the MPPT implementation [14]. The decoupled current control loop is developed to implement the current track of i_{ga_d} and i_{ga_q} and generates the *d*–*q* components v_{sa_d} and v_{sa_q} of v_{sa} in the *dq* synchronous reference frame. In order to achieve the independent control of active and reactive power from each module, v_{sa_d} and v_{sa_q} are converted to $v_{sa\_d'}$ and $v_{sa\_q'}$ in the $d'q'$ synchronous reference frame [14]. The active power from each module P_{pvja} can be obtained from the MPPT control. Therefore, the voltage $v_{ja\_d'}$ for the *j*th converter module with respect to the active power is calculated. The $v_{ja\_q'}$ related to reactive power can be obtained based on the $v_{ja\_d'}$ and (6). Consequently, the output voltage v_{ja} $(j=1,2,\ldots,n)$ from each

converter module can be synthesized. The modulation index of output voltage can be obtained by $m_{ja} = \frac{v_{ja}}{V_{\mathrm{dc}ja}}$. As a result, the active and reactive power can be properly distributed in each converter module, which achieves the MPPT and augments the security and stability of the cascaded PV system operation simultaneously.

IV. Simulation Results

In order to explore the performance of grid-interactive cascaded PV system with the proposed reactive power compensation approach, simulations were first conducted in a cosimulation platform of MATLAB/Simulink and PSIM. A 3 MW/12 kV three-phase two-stage cascaded PV system as shown in Fig. 1 is applied in this paper. The system parameters in simulation are summarized in Table II.

Figs. 11 and 12 illustrate the active and reactive power distribution, grid voltage and current change, voltage distribution among four cascaded PV converter modules with reactive power injection and absorption during different scenarios in phase a, respectively. Fig. 11(a) shows the power distribution with reactive power injection considering the low grid voltage. At the beginning, the MPPT control is enabled and each module harvests maximum power from the segmented PV arrays. At 0.5 s, the active power from four modules $P_{1a}-P_{4a}$, changes from 50 kW to 250 kW. Active power to grid P_{ga} increases from 200 MW to 1 MW. The grid current magnitude I_{ga} increases from 40 A to 200 A in Fig. 11(b). The system does not need the reactive power compensation because the symmetrical active power can equalize the output voltage from these modules. There is no overmodulation, and grid current and PCC voltage have good quality as shown in Fig. 11(b) and (c). The modulation indices from our modules, $m_{1a} - m_{4a}$, are within $[-1, 1]$. At 1 s, different active power is generated from the four modules due to the different irradiation. Modules 1 and 2 keep 250 kW active power output but the active power from modules 3 and 4 reduces to 50 kW, which results in big power fluctuation during transient. Moreover, the overmodulation caused by the unsymmetrical active power seriously distorts the grid current i_g and degrades system operation performance as shown in Fig. 11(b) and (d). The module indices from modules 1 and 2, m_{1a} and m_{2a}, are in the range $[-1, 1]$. After 1.5 s, 1 MVAR reactive power Q_{ga} is injected to grid, which means that $k_2 = -1$, and reactive power from four modules $Q_{1a}-Q_{4a}$ is controlled to the same first. It shows that the dynamic performance of reactive power is poor, which is caused by the distorted grid current and measurement module in PSIM. By the reactive power compensation, the system returns to the steady operation although active power distribution among the four modules is still unsymmetrical. P_{ga} keeps at 600 kW, which means that $k_1 = 0.6$. Once the system operates in safety and steady status, the maximum active power output from the four modules can be accurately controlled and detected. The dynamic performance of grid current, PCC voltage V_{ga}, and individual dc voltage, $V_{dc1a}-V_{dc4a}$, can be seen in Fig. 11(e). It takes 5 cycles to bring the system back to be stable. At 2 s, the reactive power from the four modules is redistributed and optimized to reduce the risk of over voltage. Fig. 11(f) shows the voltage and current waveforms before and after reactive power compensation optimization. The reactive power injection can improve system reliability but also increase the grid voltage magnitude V_{ga} from 9.7 to 10 kV. In order to limit the voltage rise, the optimized reactive power injection is reduced to -600 kVAR, that is, $k_2 = -0.6$ which is obtained from Fig. 8. In this case, the unsymmetrical reactive power is arranged between the four modules, $Q_{1a} = Q_{2a} = -95$ kVAR and $Q_{3a} = Q_{4a} = -220$ kVAR. The filter inductor loss is also provided by the PV system. By the reactive power optimization, V_{ga} decreases from 10 to 9.9 kV; the grid current still has good quality and total harmonic distortion (THD) is less than 5%. The RPCA is verified in this simulation.

Fig. 12(a) shows the power distribution with reactive power absorption considering the high grid voltage. The same active power as ones in Fig. 11 changes in each stage. At 1.5 s, 1 MVAR reactive power Q_{ga}, that is, $k_2 = 1$, is absorbed from grid to eliminate the overmodulation and $Q_{1a}-Q_{4a}$ is controlled to the same first. P_{ga} keeps at 600 kW, which means that $k_1 = 0.6$. Once the maximum active power $P_{1a}-P_{4a}$ is accurately captured at new steady system, $Q_{1a}-Q_{4a}$ is rearranged to reduce the risk of undervoltage at 2 s. The reactive power absorption can improve system reliability but also lower the grid voltage magnitude V_{ga} from 9.9 to 9.7 kV as depicted in Fig. 12(b)–(f). In order to limit the voltage drop, the total reactive power injection is reduced to 700 kVAR, that is, $k_2 = 0.7$ which is obtained from Fig. 8. In this case, optimized reactive power distribution can be derived based on (6): $Q_{1a} = Q_{2a} = 100$ kVAR and $Q_{3a} = Q_{4a} = 230$ kVAR. The filter inductor loss is provided by a grid. By the reactive power optimization, V_{ga} increases from 9.7 to 9.8 kV, good grid current is guaranteed, and THD is less than 5%.

V. Experimental Results

The experiments were conducted in the laboratory to verify the aforementioned theoretical analysis and the proposed reactive power compensation control performance. A two-stage cascaded PV system prototype with two 5 kW converter modules has been developed and the block scheme is shown in Fig. 13. The control algorithm is implemented in DSP + FPGA control platform. The downscaled circuit parameters are listed in Table III. Considering the power loss, actual line impedance and grid equivalent impedance, per units in experiments, are a little different from ones in simulations as shown in Table II.

Fig. 14 indicates active power distribution, reactive power distribution, grid voltage, and current change before and after enabling the proposed approach with reactive power injection, respectively. In the initial stage, two modules generate the same active power, $P_{1a} = P_{2a} = 710$ W, and 1.4 kW active power considering the loss is delivered to grid as shown in Fig. 14(a). The reactive power compensation is disabled because the symmetrical active power ensures the same output voltage from the two modules and stable system operation. Subsequently, P_{2a} decreases from 710 to 140 W and P_{1a} keeps 710 W, and Q_{ga} is still controlled to be zero as shown in Fig. 14(b). Therefore, the first module with $P_{1a} = 710$ W assumes more voltage

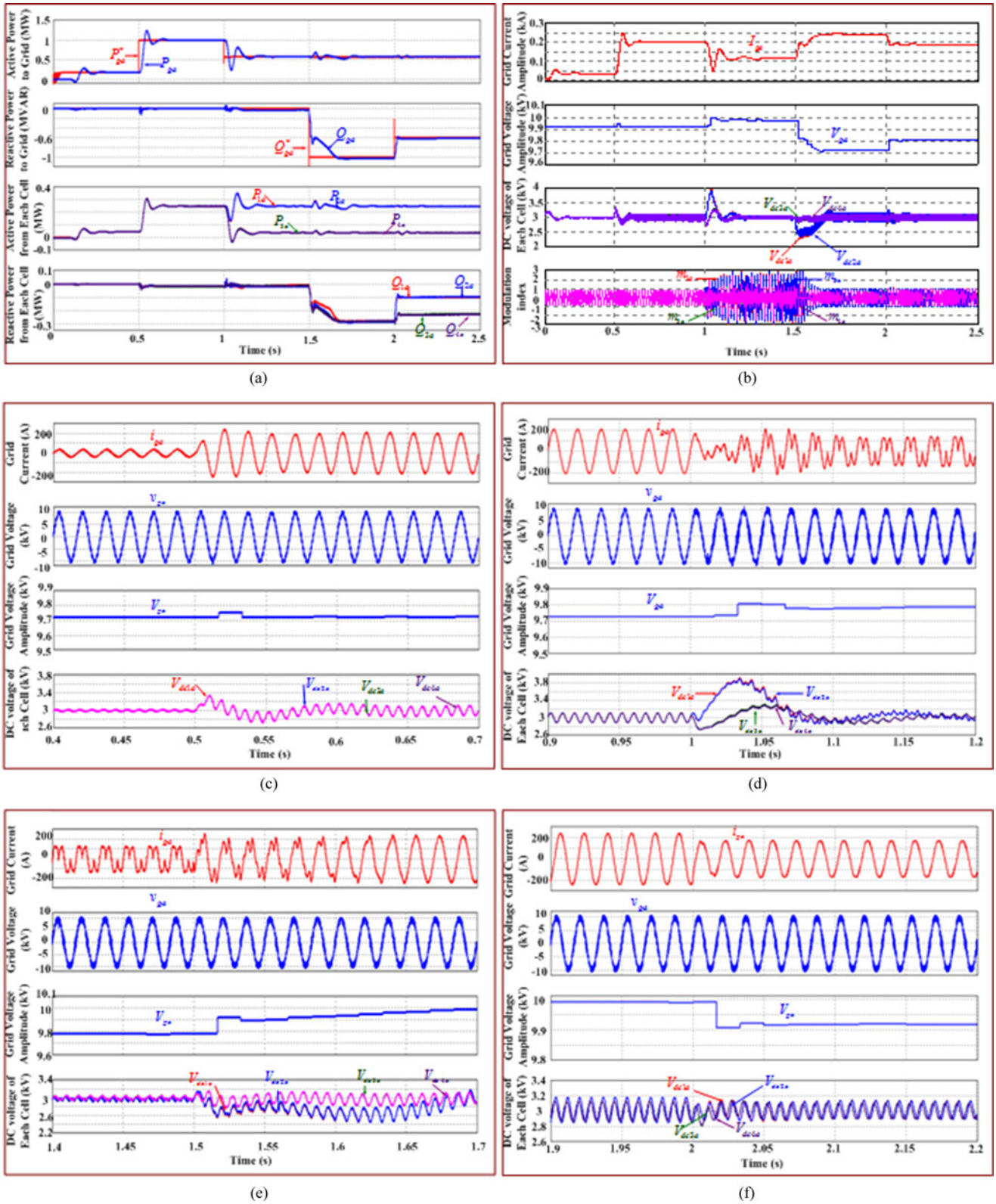

Fig. 11. Simulation results with the proposed approach in reactive power injection. (a) Active and reactive power distribution. (b) Voltage and current changes. (c) Zoomed voltage and current waveforms at 0.5 s. (d) Zoomed voltage and current waveforms at 1 s. (e) Zoomed voltage and current waveforms at 1.5 s. (f) Zoomed voltage and current waveforms at 2 s.

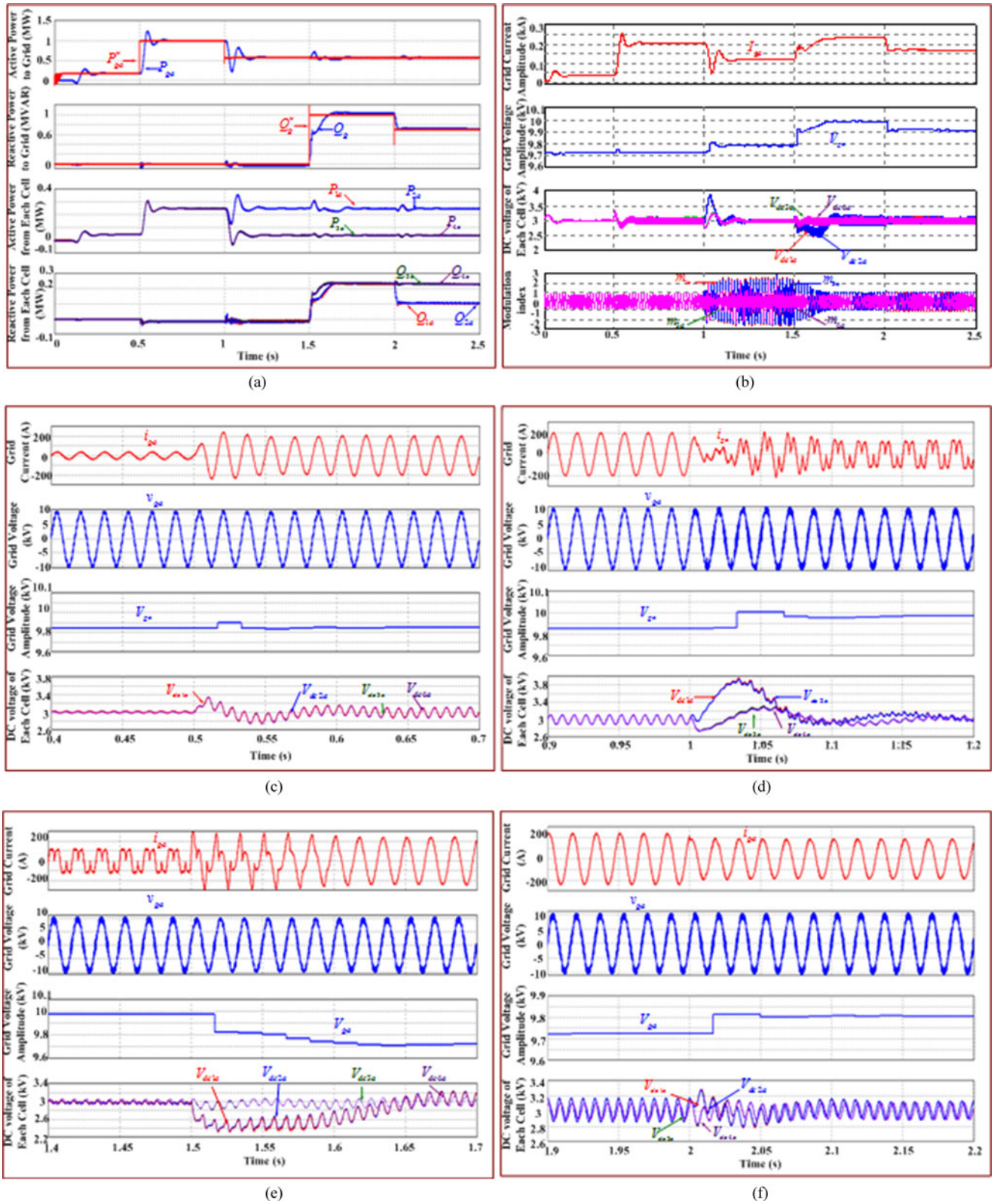

Fig. 12. Simulation results with the proposed approach in reactive power absorption. (a) Active and reactive power distribution. (b) Voltage and current changes. (c) Zoomed voltage and current waveforms at 0.5 s. (d) Zoomed voltage and current waveforms at 1 s. (e) Zoomed voltage and current waveforms at 1.5 s. (f) Zoomed voltage and current waveforms at 2 s.

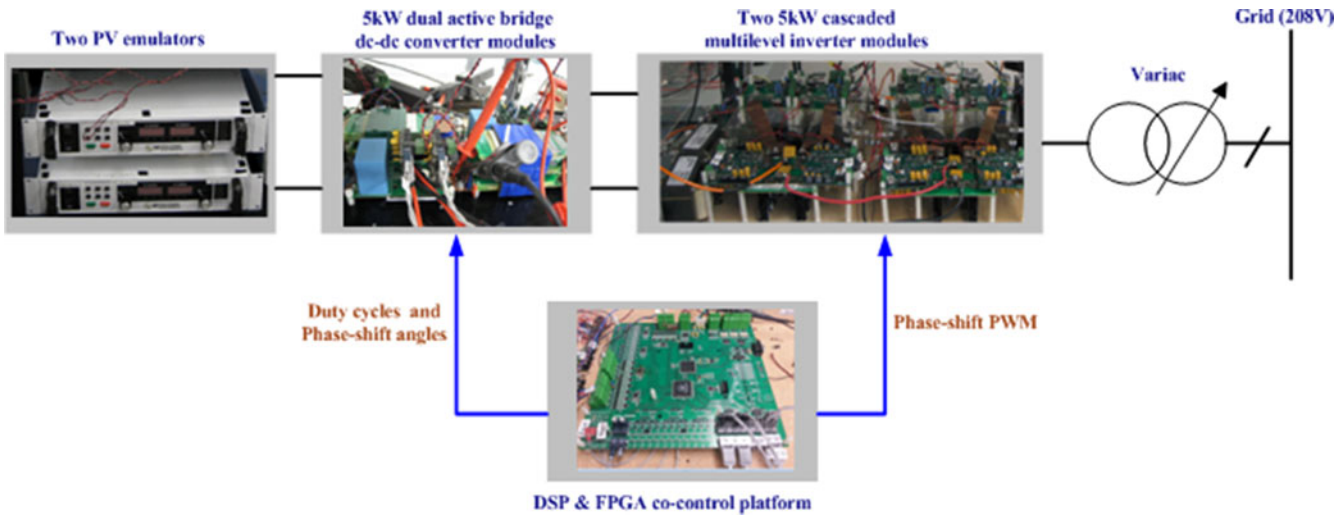

Fig. 13. Two-stage cascaded PV system prototype with two 5 kW converter modules.

TABLE III
SYSTEM CIRCUIT PARAMETERS IN EXPERIMENT

	Parameters	Symbol	Value
PV converter modules in phase a	Number	n	2
	Capacitor voltage	$V_{dcja}\,(j=1,2\ldots,n)$	200 V (0.33 p.u.)
	Capacitor size	C_{in}	400 μF (0.036 p.u.)
	Filter inductor	L_f	2 mH (0.022 p.u.)
	Switching frequency for each device	f_{SW}	10 kHz
Grid in phase a	Rated real power	P_{ga}_rated	10 kW (1.0 p.u.)
	Rated reactive power	Q_{ga}_[rated	10 kVAR (1.0 p.u.)
	RMS phase-ground voltage	v_{ga}	200 V (0.29 p.u.)

output to fulfill the system requirement, which results in overmodulation with the dc voltage limit. As a result, the grid current is distorted and serious active power mismatch will lead to the system breakdown as shown in the left zoomed waveforms of Fig. 14(c). Afterward, the proposed RPCA is activated, and maximum reactive power $Q_{ga} = -1.4$ kVAR is injected into grid and equal reactive power $Q_{1a} = Q_{2a} = -730$ VAR is generated from the two modules to eliminate the overmodulation. The loss on the filter inductor is provided by the PV system. The grid current i_{ga} retrieves good quality and THD is 4.5%. However, the -1.4 kVAR reactive power compensation incurs the grid voltage V_{ga} increase from 280 to 290 V. In order to avoid the overvoltage, the optimized reactive power compensation is introduced and Q_{ga} decreases from -1.4 to -1.1 kVAR. The reactive power distribution ratio between the two modules is 3:7 based on (6). The first module outputs high active power but provides less reactive power. The reactive power sharing does not only reduce the burden of the second module but also effectively suppresses the overmodulation. As depicted in Fig. 14(c), the V_{ga} decrease from 290 to 285 V and i_{ga} still keeps good quality.

Fig. 15 illustrates active power distribution, reactive power distribution, grid voltage, and current change before and after enabling the proposed approach with reactive power absorption, respectively. Initially, two modules generate the same active power, $P_{1a} = P_{2a} = 760$ W, and 1.5 kW active power considering the loss is delivered to grid as shown in Fig. 15(a). The reactive power compensation is disabled in Fig. 15(b). Subsequently, P_{2a} decreases from 760 to 150 W and P_{1a} keeps 760 W, and Q_{ga} is still controlled to be zero, which causes serious grid current distortion as shown in the left zoomed waveforms of Fig. 15(c). In order to ensure the safe and stable system operation, the maximum reactive power $Q_{ga} = 1.45$ kVAR is first absorbed from grid and the same reactive power $Q_{1a} = Q_{2a} = 700$ VAR is absorbed by the two modules as shown in Fig. 15(b). The loss on the filter inductor is provided by grid. The i_{ga} recovers good quality and THD is 4.68%. However, the 1.45 kVAR reactive power compensation incurs the grid voltage V_{ga} decrease from 300 to 285 V. In order to avoid the undervoltage, the optimized reactive power compensation is enabled and Q_{ga} decreases from 1.45 to 1.15 kVAR. The reactive power distribution ratio between the two modules is 3:7 based on (6). The

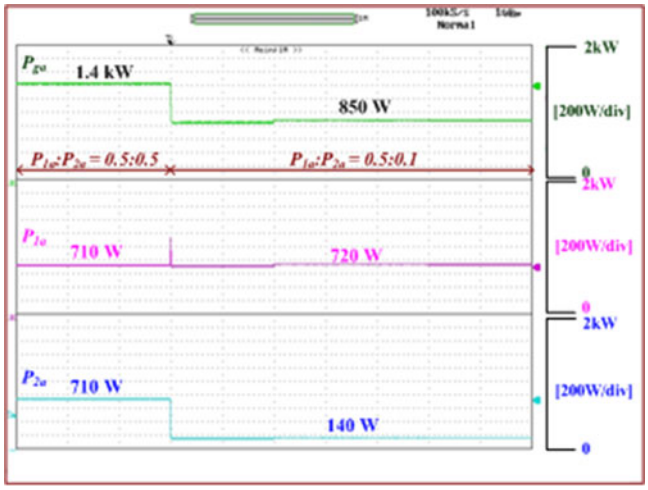

(a)

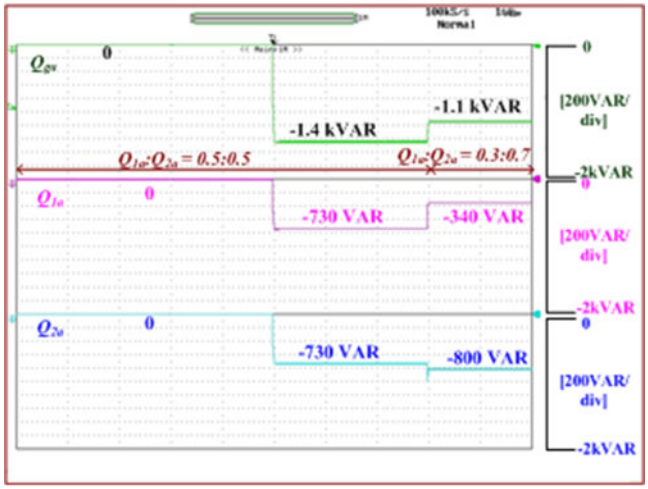

(b)

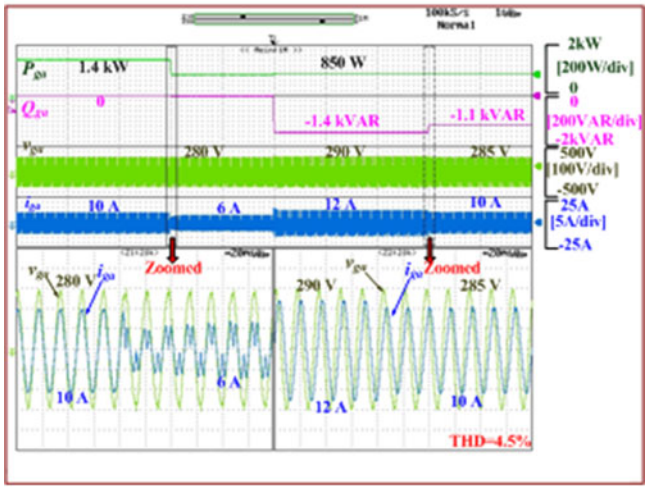

(c)

Fig. 14. Experimental results with the proposed approach in reactive power compensation injection. (a) Active power distribution. (b) Reactive power distribution. (c) Voltage and current waveforms with and without reactive power compensation.

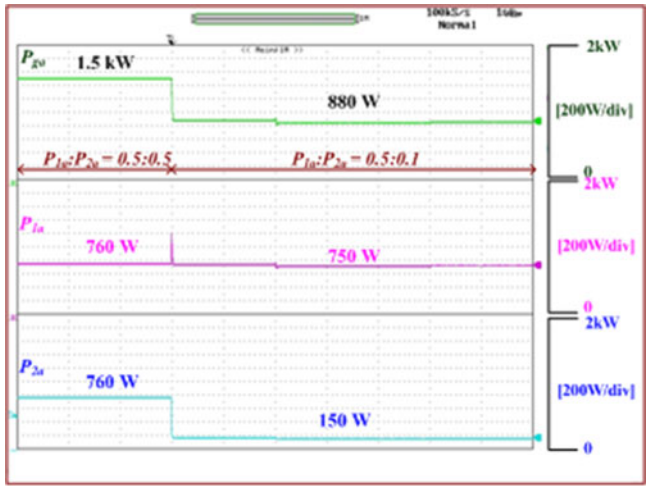

(a)

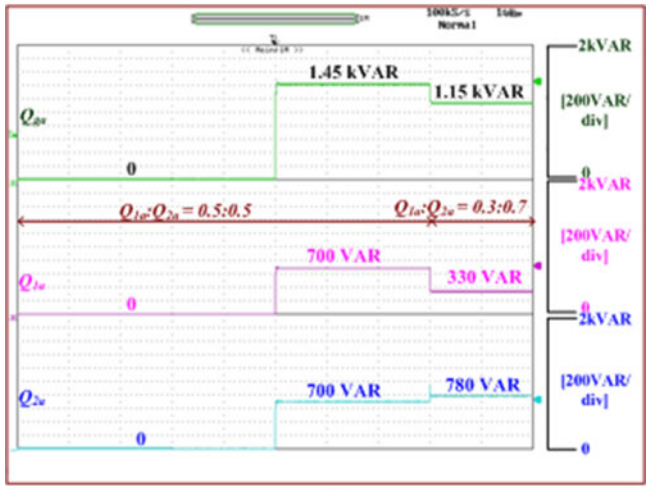

(b)

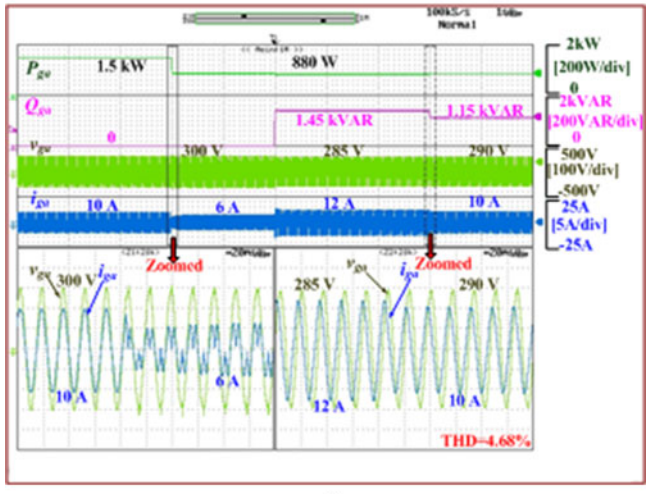

(c)

Fig. 15. Experimental results with the proposed approach in reactive power absorption. (a) Active power distribution. (b) Reactive power distribution. (c) Voltage and current waveforms with and without reactive power compensation.

first module with high active power shares less reactive power generation, which contributes on undervoltage elimination and system reliability. It can be seen from Fig. 15(c) that V_{ga} increase from 285 to 290 V and i_{ga} still maintains good quality.

The previous experimental results are consistent with the simulation results shown in Figs. 10 and 11.

VI. Conclusion

This paper addressed the effect of reactive power compensation on system operation performance in grid-interactive cascaded PV systems. The system stability and reliability issue caused by unsymmetrical active power was specifically analyzed. Reactive power compensation and distribution was introduced to mitigate this issue. The output voltage of each module was verified to directly determine the power distribution. The relationship between voltage distribution and power distribution was illustrated with a wide power change range. An optimized RPCA was proposed considering the MPPT implementation, grid voltage, and overmodulation. Moreover, the RPAC was eligible to be integrated into different types of the cascaded PV system. Correspondingly, the control system with MPPT control and optimized RPCA was developed and validated by the simulation and experimental results under different scenarios. The proposed approach was demonstrated to be able to effectively enhance system operation stability and reliability, and improve power quality.

References

[1] Y. Bo, L. Wuhua, Z. Yi, and H. Xiangning, "Design and analysis of a grid connected photovoltaic power system," *IEEE Trans. Power Electron.*, vol. 25, no. 4, pp. 992–1000, Apr. 2010.

[2] J. Ebrahimi, E. Babaei, and G. B. Gharehpetian, "A new topology of cascaded multilevel converters with reduced number of components for high-voltage applications," *IEEE Trans. Power Electron.*, vol. 26, no. 11, pp. 3109–3118, Nov. 2011.

[3] L. Nousiainen and J. Puukko, "Photovoltaic generator as an input source for power electronic converters," *IEEE Trans. Power Electron.*, vol. 28, no. 6, pp. 3028–3037, Jun. 2013.

[4] D. Meneses, F. Blaabjery, O. Garcia, and J. A. Cobos, "Review and comparison of step-up transformerless topologies for photovoltaic ac-module application," *IEEE Trans. Power Electron.*, vol. 28, no. 6, pp. 2649–2663, Jun. 2013.

[5] Y. Zhou, H. Li, and L. Liu, "Integrated autonomous voltage regulation and islanding detection for high penetration PV applications," *IEEE Trans. Power Electron.*, vol. 28, no. 6, pp. 2826–2841, Jun. 2013.

[6] J. Mei, B. Xiao, K. Shen, L. M. Tolbert, and J. Y. Zheng, "Modular multilevel inverter with new modulation method and its application to photovoltaic grid-connected generator," *IEEE Trans. Power Electron.*, vol. 28, no. 11, pp. 5063–5073, Nov. 2013.

[7] Y. Zhou, L. Liu, and H. Li, "A high performance photovoltaic module-integrated converter (MIC) based on cascaded quasi-Z-source inverters (qZSI) using eGaN FETs," *IEEE Trans. Power Electron.*, vol. 28, no. 6, pp. 2727–2738, Jun. 2013.

[8] L. Liu, H. Li, and Y. Zhou, "A cascaded photovoltaic system integrating segmented energy storages with self-regulating power distribution control and wide range reactive power compensation," *IEEE Trans. Power Electron.*, vol. 26, no. 12, pp. 3545–3559, Dec. 2011.

[9] Q. Li and P. Wolfs, "A review of the single phase photovoltaic module integrated converter topologies with three different dc link configurations," *IEEE Trans. Power Electron.*, vol. 23, no. 3, pp. 1320–1333, May 2008.

[10] L. Zhang, K. Sun, Y. Xing, L. Feng, and H. Ge, "A modular grid-connected photovoltaic generation system based on dc bus," *IEEE Trans. Power Electron.*, vol. 26, no. 2, pp. 523–531, Feb. 2011.

[11] L. M. Tolbert and F. Z. Peng, "Multilevel converters as a utility interface for renewable energy systems," in *Proc. IEEE Power Eng. Soc. Summer Meeting*, Seattle, WA, Jul. 2000, pp. 1271–1274.

[12] M. R. Islam, Y. Guo, and J. Zhu, "A high-frequency link multilevel cascaded medium-voltage converter for direct grid integration of renewable energy systems," *IEEE Trans. Power Electron.*, vol. 29, no. 8, pp. 4167–4182, Aug. 2014

[13] S. Harb and R. S. Balog, "Reliability of candidate photovoltaic module-integrated-inverter (PV-MII) topologies—A usage model approach," *IEEE Trans. Power Electron.*, vol. 28, no. 6, pp. 3019–3027, Jun. 2013.

[14] L. Liu, H. Li, and Y. Xue "A coordinated active and reactive power control strategy for grid-connected cascaded photovoltaic (PV) system in high voltage high power applications," in *Proc. 28th IEEE Appl. Power Electron. Conf. Expo.*, Long Beach, CA, Mar. 17–21, 2013, pp. 1301–1308.

[15] K. Corzine and Y. Familiant, "A new cascaded multilevel H-bridge drive," *IEEE Trans. Power Electron.*, vol. 17, no. 1, pp. 125–131, Jan. 2002.

[16] J. Wang and F. Z. Peng, "Unified power flow controller using the cascade multilevel inverter," *IEEE Trans. Power Electron.*, vol. 19, no. 4, pp. 1077–1084, Jul. 2004.

[17] B. P. McGrath and D. G. Holmes, "Natural capacitor voltage balancing for a flying capacitor converter induction motor drive," *IEEE Trans. Power Electron.*, vol. 24, no. 6, pp. 1554–1561, Jun. 2009.

[18] Q. Song and W. Liu, "Control of a cascade STATCOM with star configuration under unbalanced conditions," *IEEE Trans. Power Electron.*, vol. 24, no. 1, pp. 45–58, Jan. 2009.

[19] C. D. Townsend, T. J. Summers, and R. E. Betz, "Multigoal heuristic model predictive control technique applied to a cascaded H-bridge StatCom," *IEEE Trans. Power Electron.*, vol. 27, no. 3, pp. 1191–1200, Mar. 2012.

[20] K. Sano and M. Takasaki, "A transformerless D-STATCOM based on a multivoltage cascaded converter requiring no dc source," *IEEE Trans. Power Electron.*, vol. 27, no. 6, pp. 2783–2795, Jun. 2012.

[21] C. D. Townsend, T. J. Summers, J. Vodden, A. J. Watson, R. E. Betz, and J. C. Clare, "Optimization of switching losses and capacitor voltage ripple using model predictive control of a cascaded H-bridge multilevel StatCom," *IEEE Trans. Power Electron.*, vol. 28, no. 7, pp. 3077–3087, Jul. 2013.

[22] S. Du, J. Liu, J. Lin, and Y. He, "A novel dc voltage control method for STATCOM based on hybrid multilevel H-bridge converter," *IEEE Trans. Power Electron.*, vol. 28, no. 1, pp. 101–111, Jan. 2013.

[23] B. Gultekin and M. Ermis, "Cascaded multiulevel converter-based transmission STATCOM: System design methodology and development of a 12 kV $\pm$ 12 MVAr power stage," *IEEE Trans. Power Electron.*, vol. 28, no. 11, pp. 4930–4950, Nov. 2013.

[24] M. Hagiwara, K. Nishimura, and H. Akagi, "A medium-voltage motor drive with a modular multilevel PWM inverter," *IEEE Trans. Power Electron.*, vol. 25, no. 7, pp. 1786–1799, Jul. 2010.

[25] J. Rodriguez, J. S. Lai, and F. Z. Peng, "Multilevel inverters: A survey of topologies, controls, and applications," *IEEE Trans. Ind. Appl.*, vol. 49, no. 4, pp. 724–738, Aug. 2002.

[26] T. Zhao, G. Wang, S. Battacharya, and A. Q. Huang, "Voltage and power balance control for a cascaded H-bridge converter-based solid-state transformer," *IEEE Trans. Power Electron.*, vol. 28, no. 4, pp. 1523–1532, Apr. 2013.

[27] X. She, A. Q. Huang, and X. Ni, "Current sensorless power balance strategy for dc/dc converters in a cascaded multilevel converter based solid state transformer," *IEEE Trans. Power Electron.*, vol. 29, no. 1, pp. 17–22, Jan. 2014.

[28] S. Du, J. Liu, and J. Lin, "Hybrid cascaded H-bridge converter for harmonic current compensation," *IEEE Trans. Power Electron.*, vol. 28, no. 5, pp. 2170–2179, May 2013.

[29] C. F. Ciancetta and P. Siano, "A multilevel inverter for photovoltaic systems with fuzzy logic control," *IEEE Trans. Ind. Electron.*, vol. 57, no. 12, pp. 4115–4125, Dec. 2010.

[30] E. Villanueva, P. Correa, J. Rodriguez, and M. Pacas, "Control of a single-phase cascaded H-bridge multilevel inverter for grid-connected photovoltaic systems," *IEEE Trans. Ind. Electron.*, vol. 56, no. 11, pp. 4399–4406, Sep. 2009.

[31] O. Alonso, P. Sanchis, E. Gubia, and L. Marroyo, "Cascaded H-bridge multilevel converter for grid connected photovoltaic generators with independent maximum power point tracking of each solar array," in *Proc. 34th Annu. IEEE Power Electron. Spec. Conf.*, Jun. 2003, vol. 2, pp. 731–735.

[32] Y. Xu, L. M. Tolbert, J. N. Chiasson, F. Z. Peng, and J. B. Campbell, "Generalized instantaneous non-active power theory for STATCOM," *IET Electr. Power Appl.*, vol. 1, no. 6, pp. 853–861, Nov. 2007.
[33] M. Rezaei, H. Iman-Eini, and S. Farhangi, "Grid-connected photovoltaic system based on a cascaded H-Bridge inverter," *J. Power Electron.*, vol. 12, no. 4, pp. 578–86, Jul. 2002.
[34] Y. Shi, L. Liu, H. Li, and Y. Xue, "A single-phase grid-connected PV converter with minimal dc-link capacitor and low-frequency ripple-free maximum power point tracking," in *Proc. 5th IEEE Energy Convers. Congr. Expo.*, Denver, CO, Sep. 15–19, 2013, pp. 2385–2390.
[35] L. Liu, H. Li, Y. Xue, and W. Liu, "Decoupled active and reactive power control for large scale grid-connected photovoltaic systems using cascaded modular multilevel converter," to be published *IEEE Trans. Power Electron.* 2014.
[36] D. Aquila, M. Liserre, V. G. Monopoli, and P. Rotondoi, "Overview of PI-based solutions for the control of dc buses of a single-phase H-bridge multilevel active rectifier," *IEEE Trans. Ind. Appl.*, vol. 44, no. 3, pp. 857–866, May/Jun. 2008.

Liming Liu (M'09–SM'11) received the B.S. and M.S. degrees from Wuhan University, Wuhan, China, in 1998 and 2003, respectively, and the Ph.D. degree from the Huazhong University of Science and Technology, Wuhan, in 2006, all in electrical engineering.

He joined the Center for Advanced Power Systems, Florida State University, Tallahassee, FL, USA, in 2007 as a Postdoctoral Researcher, where he was an Assistant Scientist from 2008 to 2013. He is currently a Senior Scientist at ABB, Inc., Raleigh, NC, USA. His research interests generally include wide band gap devices investigation and application, medium/high voltage dc voltage converter, modeling and control of multilevel inverter applications, renewable energy conversion systems, high penetrative grid-interactive photovoltaic system, smart grid, motor drive control with hybrid energy storages, and flexible ac transmission system.

Hui Li (S'97–M'00–SM'01) received the B.S. and M.S. degrees from the Huazhong University of Science and Technology, Wuhan, China, in 1992 and 1995, respectively, and the Ph.D. degree from the University of Tennessee, Knoxville, USA, in 2000, all in electrical engineering.

She is currently a Full Professor in the Electrical and Computer Engineering Department at the Florida A&M University–Florida State University College of Engineering, Tallahassee, FL, USA. Her research interests include bidirectional dc–dc converters, cascaded multilevel inverters, and power electronics application in hybrid electric vehicles.

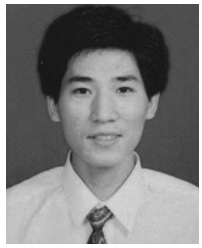

Yaosuo Xue (M'03–SM'12) received the B.Sc. degree in electrical engineering from East China Jiaotong University, Nanchang, China, in 1991, and the M.Sc. degree in electrical engineering from the University of New Brunswick, Fredericton, NB, Canada, in 2004, where he is currently working toward the Ph.D. degree.

During 2005 to 2006, he was with Capstone Turbine Corp., CA, USA, as a Lead Power Electronics and Systems Engineer developing advanced microturbine systems. Since 2009, he has been a Research Scientist and currently Research Project Manager at Corporate Technology, Siemens Corporation, Princeton, NJ, USA, where he cofounded the Siemens Corporate Technology's power electronics research group in USA.

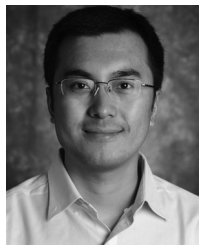

Wenxin Liu (S'01–M'05) received the B.S. and M.S. degrees from Northeastern University, Shenyang, China, in 1996 and 2000, respectively, and the Ph.D. degree in electrical engineering from the Missouri University of Science and Technology (the formerly University of Missouri-Rolla), Rolla, MO, USA, in 2005.

Then, he worked as an Assistant Scholar Scientist with the Center for Advanced Power Systems of Florida State University until 2009. From 2009 to 2014, he was an Assistant Professor with the Klipsch School of Electrical and Computer Engineering of New Mexico State University, Las Cruces, NM, USA. Currently, he is an Assistant Professor with the Department of Electrical and Computer Engineering of Lehigh University, Bethlehem, PA, USA. His research interests include power systems, power electronics, and controls.